Three-Dimensional Pattern Formations in a Biological Model of Chemotaxis and Growth

Takayuki Narumi and Koichi Osaki

Graduate School of Science and Technology, Kwansei Gakuin University

1 Introduction

Many living matters rely on taxis, that is, movement responsive to a stimulus such as temperature, light, or a chemical. Here, we consider a directed motion induced by a chemical, so-called chemotaxis. Chemotaxis has been studied mathematically in numerous PDE models (see Ref. [3] and references therein). In particular, we study a model of chemotaxis and growth, introduced by Mimura and Tsujikawa [5]:

$$\begin{cases} \partial u/\partial t &= D\Delta u - a\nabla \cdot (u\nabla\rho) + ru(1-u) & \text{in} \quad \Omega \times (0,\infty), \\ \partial \rho/\partial t &= \Delta\rho + fu - g\rho & \text{in} \quad \Omega \times (0,\infty), \\ \partial u/\partial \nu &= \partial\rho/\partial\nu = 0 & \text{on} \quad \partial\Omega \times (0,\infty), \end{cases} \quad (1.1)$$

where Ω is a bounded domain in $\mathbb{R}^d$ with boundary $\partial\Omega$, and ν denotes the outward normal vector on the boundary. The coefficients D, a, r, f, and g are positive constants. The unknown functions of the model are the population density $u = u(\boldsymbol{x}, t)$ of a living matter and the density $\rho = \rho(\boldsymbol{x}, t)$ of a chemical substance. The initial conditions are $u(\boldsymbol{x}, 0) = u_0(\boldsymbol{x})$ and $\rho(\boldsymbol{x}, 0) = \rho_0(\boldsymbol{x})$ in Ω. The living matter directs its motion up a gradient of ρ, and produces the chemical substance. The chemical substance decomposes linearly. The general conservation equation for $u(\boldsymbol{x}, t)$ is $\partial_t u + \nabla \cdot \boldsymbol{J} = f(u)$, where $f(u)$ denotes the growth of u. The flux $\boldsymbol{J}$ includes the normal diffusion and the chemotaxis: $\boldsymbol{J} = \boldsymbol{J}_{\text{diff}} + \boldsymbol{J}_{\text{taxis}}$. These contributions are $\boldsymbol{J}_{\text{diff}} = -D\nabla u$ with the diffusion constant D, and $\boldsymbol{J}_{\text{taxis}} = u\chi(\rho)\nabla\rho$ with the chemotactic factor $\chi(\rho)$. If the living matter is assumed to grow logistically and $\chi(\rho)$ is a constant, the model (1.1) is obtained.

A nonlinear effect such as the taxis induces spatial pattern formations. The pattern in the model (1.1) emerges due to the competition of spatial expansion and contraction of u. In the case of $a = 0$, u and ρ are independent of each other, and the equation of u reduces to the Fisher–Kolmogorov equation, which has traveling wavefront solutions. In the case of $r = 0$, on the other hand, the model (1.1) is equivalent to the classical Keller–Segel model, which has blow-up solutions with a δ-function singularity. We can intuitively regard a and r as control parameters of contraction and expansion, respectively. Several interesting spatial patterns have been obtained in chemotaxis models. However, most are one-dimensional (1D) or two-dimensional (2D) patterns, while there are few theoretical studies for three-dimensional (3D) cases [8, 9]. 3D patterns in other models also have been investigated in detail because of the difficulty observing 3D patterns in experiments, although this is being rectified now by the use of innovative equipment such as tomographs [1]. Therefore, the study of 3D patterns needs

to advance; the present paper focuses on 3D pattern formations in the chemotaxis and growth model (1.1). Kuto et al. [4] have analyzed the 2D model and shown the existence of hexagonal patterns represented by the superposition of multiple cosine modes. We then expect that the 3D model has solutions that exhibit cubic-crystal patterns as a superposition of cosine modes. We first review the local bifurcation analysis by Kuto et al. [4], and show the results of 2D and 3D numerical calculations.

2 Preliminaries

We consider the stationary problem of the model (1.1):

$$
\begin{cases}
D\Delta u - a\nabla \cdot (u\nabla\rho) + ru(1-u) & = 0 \quad \text{in } \Omega, \\
\Delta\rho + fu - g\rho & = 0 \quad \text{in } \Omega, \\
\partial u/\partial\nu = \partial\rho/\partial\nu = 0 & \quad \text{on } \partial\Omega.
\end{cases}
\tag{2.1}
$$

Kuto et al. [4] verified that hexagonal patterns emerge in the 2D case of (2.1). We briefly review their results in this section.

2.1 bifurcation points of 2D patterns

By considering the dual periodicity of hexagons, the domain Ω is assumed to be the rectangle $\Omega_{\mathrm{r}} = (0, L) \times \left(0, L/\sqrt{3}\right)$, where $L > 0$. We introduce a Hilbert space with Neumann boundary condition $H_\nu^2(\Omega_{\mathrm{r}}) = \{w \in H^2(\Omega_{\mathrm{r}}) : \partial w/\partial\nu = 0 \text{ on } \partial\Omega_{\mathrm{r}}\}$. Associated with (2.1), a nonlinear operator $F : H_\nu^2(\Omega_{\mathrm{r}}) \times H_\nu^2(\Omega_{\mathrm{r}}) \times \mathbb{R} \rightarrow L^2(\Omega) \times L^2(\Omega)$ is defined as

$$
F(u, \rho, a) = \begin{pmatrix} D\Delta u - a\nabla \cdot (u\nabla\rho) + ru(1-u) \\ \Delta\rho + fu - g\rho \end{pmatrix}.
\tag{2.2}
$$

Here $a \in \mathbb{R}$ is a bifurcation parameter. We consider the linearized problem around a trivial solution $(u, \rho) = (1, f/g)$:

$$
F_{(u,\rho)}(a) \begin{pmatrix} u_\delta \\ \rho_\delta \end{pmatrix} = \begin{pmatrix} D\Delta u_\delta - a\Delta\rho_\delta - ru_\delta \\ \Delta\rho_\delta + fu_\delta - g\rho_\delta \end{pmatrix} = \mathbf{0}.
\tag{2.3}
$$

From the Neumann boundary condition, solutions of (u_δ, ρ_δ) are represented by the Fourier series expansion $u_\delta = \sum_{\boldsymbol{n}} \tilde{u}_{\boldsymbol{n}}\Phi_{\boldsymbol{n}}(\boldsymbol{x})$ and $\rho_\delta = \sum_{\boldsymbol{n}} \tilde{\rho}_{\boldsymbol{n}}\Phi_{\boldsymbol{n}}(\boldsymbol{x})$, where

$$
\Phi_{\boldsymbol{n}}(\boldsymbol{x}) = \cos\left(\frac{\pi n_x x}{L}\right) \cos\left(\frac{\sqrt{3}\pi n_y y}{L}\right).
\tag{2.4}
$$

Each element of $\boldsymbol{n} = (n_x, n_y)$ is a non-negative integer. Note that the amplitudes $\tilde{u}_{\boldsymbol{n}}$ and $\tilde{\rho}_{\boldsymbol{n}}$ are zero for $\boldsymbol{n} = \mathbf{0}$. Equation (2.3) has nontrivial solutions if and only if

$$
\begin{vmatrix} -\left(D\hat{n}^2 + r\right) & a\hat{n}^2 \\ f & -\left(\hat{n}^2 + g\right) \end{vmatrix} = 0 \quad \Leftrightarrow \quad a = \frac{\left(D\hat{n}^2 + r\right)\left(\hat{n}^2 + g\right)}{f\hat{n}^2} := a_{\mathrm{c}}(\boldsymbol{n}),
\tag{2.5}
$$

where $\hat{n}^2 = \pi^2(n_x^2 + 3n_y^2)/L^2$. When $a = a_{\mathrm{c}}(\boldsymbol{n})$, the bifurcation of corresponding modes can emerge. Some modes have the same value of $a_{\mathrm{c}}(\boldsymbol{n})$. Multiple degenerate bifurcations can produce complex patterns such as hexagons.

2.2 local bifurcation analysis

For the rectangular domain Ω_r, Kuto et al. [4] carried out the local bifurcation theory of Crandall and Rabinowitz [2].

Theorem 2.1 *(Theorem 5.1 in Ref. [4]). If* $\dim \operatorname{Ker} F_{(u,\rho)}(a_c) = 1$, *there exists a positive constant* δ *such that non-constant solutions of (2.1) near* $(u, \rho, a) = (1, f/g, a_c) \in H_\nu^2(\Omega_r) \times H_\nu^2(\Omega_r) \times \mathbb{R}$ *can be represented by*

$$
\begin{pmatrix} u(s) \\ \rho(s) \\ a(s) \end{pmatrix} = \begin{pmatrix} 1 \\ f/g \\ a_c(\boldsymbol{n}) \end{pmatrix} + s \begin{pmatrix} \Phi_{\boldsymbol{n}}(\boldsymbol{x}) \\ k\Phi_{\boldsymbol{n}}(\boldsymbol{x}) \\ \beta \end{pmatrix} + s^2 \begin{pmatrix} u_{\mathrm{h}}(s) \\ \rho_{\mathrm{h}}(s) \\ a_{\mathrm{h}}(s) \end{pmatrix} \tag{2.6}
$$

with $\beta = 0$ *for all* $s \in [-\delta, \delta]$. *Here* $\Phi_{\boldsymbol{n}}(\boldsymbol{x})$ *is defined in (2.4),* $k = f \big/ \big(\hat{n}^2 + g\big)$, *and* $(u_{\mathrm{h}}(s), \rho_{\mathrm{h}}(s), a_{\mathrm{h}}(s)) \in H_\nu^2(\Omega_r) \times H_\nu^2(\Omega_r) \times \mathbb{R}$ *is a smooth function of s.*

This theorem implies that, if $n_x = 0$ or $n_y = 0$, the stripe solutions bifurcate at a_c, or otherwise the rectangle solutions bifurcate at a_c.

The simplest pattern of threefold symmetry is represented by two cosine modes:

$$
\Psi(\boldsymbol{x}) = \cos\left(\frac{2\pi x}{L}\right) + 2\cos\left(\frac{\pi x}{L}\right)\cos\left(\frac{\sqrt{3}\pi y}{L}\right). \tag{2.7}
$$

This is the superposition of modes $(2, 0)$ and $(1, 1)$ of (2.4), where those solutions bifurcate at the same a_c. The hexagonal pattern is represented by $c\Psi(\boldsymbol{x})$ with a negative constant c. Since $\dim \operatorname{Ker} F_{(u,\rho)}(a_c(2,0)) > 1$, we cannot apply Theorem 2.1 for the bifurcation of the threefold-symmetry pattern. Kuto et al. [4] introduced a closed subspace of threefold symmetry H_{hex}^2 of $H_\nu^2(\Omega_r)$ according to Ref. [6], and showed the local bifurcation of hexagonal patterns.

Theorem 2.2 *(Theorems 6.1 and 6.2 in Ref. [4]). There exist a positive constant* δ *and a neighborhood* O_{hex} *of* $(u, \rho, a) = (1, f/g, a_c(2,0))$ *in* $H_{\mathrm{hex}}^2 \times H_{\mathrm{hex}}^2 \times \mathbb{R}$ *such that non-constant solutions of (2.1) contained in* O_{hex} *can be represented by*

$$
\begin{pmatrix} u(s) \\ \rho(s) \\ a(s) \end{pmatrix} = \begin{pmatrix} 1 \\ f/g \\ a_c(2,0) \end{pmatrix} + s \begin{pmatrix} \Psi(\boldsymbol{x}) \\ k\Psi(\boldsymbol{x}) \\ \beta \end{pmatrix} + s^2 \begin{pmatrix} u_{\mathrm{h}}(s) \\ \rho_{\mathrm{h}}(s) \\ a_{\mathrm{h}}(s) \end{pmatrix} \tag{2.8}
$$

with

$$
\beta = \frac{4\pi^2 + gL^2}{8\pi^2 f}\left(r - \frac{4\pi^2 D}{L^2}\right) \tag{2.9}
$$

for $s \in [-\delta, \delta]$. *Here* $\Psi(\boldsymbol{x})$ *is defined in (2.7),* $k = fL^2 \big/ \big(4\pi^2 + gL^2\big)$, *and* $(u_{\mathrm{h}}(s), \rho_{\mathrm{h}}(s), a_{\mathrm{h}}(s)) \in H_{\mathrm{hex}}^2 \times H_{\mathrm{hex}}^2 \times \mathbb{R}$ *is a smooth function of s.*

Remarkably, β is zero for the stripe and rectangle solutions, but not generally zero for the solutions of threefold symmetry. This implies that the bifurcation to the stripe and rectangle patterns is pitchfork type and that to the hexagonal patterns is generically transversal type. Further, (2.8) and (2.9) suggest the existence of either a pattern $u_\delta \approx s\Phi_{\boldsymbol{n}}(\boldsymbol{x})$ or its inverse pattern $u_\delta \approx -s\Phi_{\boldsymbol{n}}(\boldsymbol{x})$ near the bifurcation point. We discuss it later by numerical calculations.

3 Bifurcation to cubic-crystal patterns

We next explore the emergence of crystal-like patterns in the 3D chemotaxis and growth model (1.1). In the present paper, our focus is cubic crystals, i.e., simple cubic (SC), face-centered cubic (FCC), and body-centered cubic (BCC) patterns. The domain is the cube $\Omega_c = (0, L) \times (0, L) \times (0, L)$, where $L > 0$. For the 3D case, we can also apply the result of Sec. 2.1, while the basis of Fourier series expansion is

$$\Phi_n(x) = \cos(\pi n_x x/L) \cos(\pi n_y y/L) \cos(\pi n_z z/L) \tag{3.1}$$

instead of (2.4), and moreover (2.5) holds with $\hat{n}^2 = \pi^2(n_x^2 + n_y^2 + n_z^2)/L^2$.

The cubic-crystal patterns are expressed by cosine modes. The FCC pattern has the same symmetry as the mode $(1, 1, 1)$, i.e., $\Phi_{(1,1,1)}(x)$. Since $\dim \operatorname{Ker} F_{(u,\rho)}(a_c(1, 1, 1)) = 1$, we can apply the local bifurcation theory for the existence of the non-constant solution. The BCC and SC patterns cannot be expressed by a single cosine mode. The BCC pattern is represented by the superposition of $\Phi_{(1,1,0)}(x)$, $\Phi_{(1,0,1)}(x)$, and $\Phi_{(1,1,0)}(x)$. Similarly, the SC pattern is the superposition of $\Phi_{(1,0,0)}(x)$, $\Phi_{(0,1,0)}(x)$, and $\Phi_{(0,0,1)}(x)$. The BCC and SC patterns are therefore 3D degenerate: $\dim \operatorname{Ker} F_{(u,\rho)}(a_c(1, 1, 0)) = \dim \operatorname{Ker} F_{(u,\rho)}(a_c(1, 0, 0)) = 3$. We thus cannot apply the local bifurcation theory directly for BCC and SC. Nevertheless, as with the 2D case, one can carry out the local bifurcation analysis in an appropriately restricted function space to prove that the bifurcation to the SC and FCC patterns is pitchfork type (i.e., $\beta = 0$) and that the bifurcation to the BCC pattern is transversal type (i.e., $\beta \neq 0$). We do not mention the details here, but show numerical results in the next section.

4 Numerical solutions

4.1 method

We carried out a numerical calculation for the model (1.1). The control parameters were a and r; the other parameters were set as those in Ref. [4]: $D = 0.0625$, $f = 1$, and $g = 32$. The initial function $u_0(x)$ included the perturbation $\xi(x)$ around the constant solution: $u_0(x) = 1 + \xi(x)$, where the value of $\xi(x)$ was random number in the uniform distribution between -0.05 and 0.05. The function $\rho_0(x)$ was constant: $\rho_0(x) = f/g = 0.03125$. We employed the explicit numerical scheme in time. The spatial-derivative terms were approximated by the central difference. The grid sizes were $\Delta x = \Delta y = \Delta z = 2^{-5}$ in space and $\Delta t = 2^{-15}$ in time. The simulation continues to a steady state.

4.2 result and discussion

4.2.1 2D: hexagonal pattern

The domain in this case was $\Omega_{r,4} = (0, 4L) \times \left(0, 4L/\sqrt{3}\right)$. The system size L was determined to obtain the hexagonal pattern at the first bifurcation. It is proved that $a_c(n) \geq \left(\sqrt{r} + \sqrt{Dg}\right)^2 \big/ f := a_{\min}$, where $a_{\min}$ is attained at $L = \pi |n| (D/rg)^{1/4}$ with $|n|^2 = n_x^2 + 3n_y^2$.
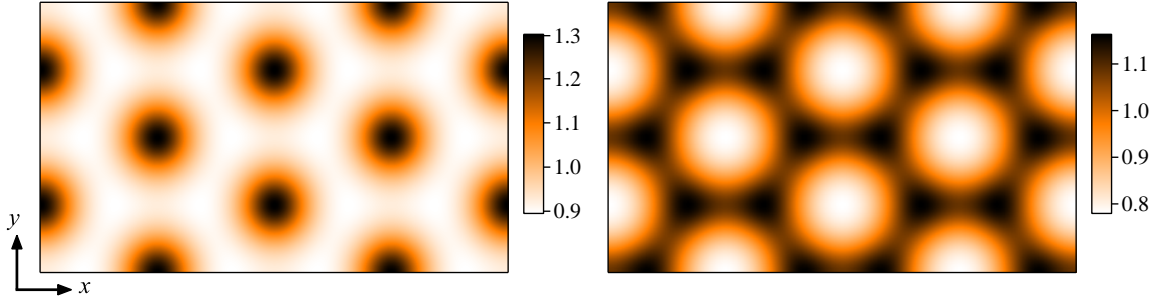
Figure 1: 2D steady-state patterns of dots (left) and hexagons (right) in $\Omega_{r,4}$. The parameter r was $r = 1.5$ (left) and $r = 3.5$ (right), while a was adjusted to $(a - a_c)/a_c = 0.01$. The length L was set to obtain each pattern as the first bifurcation; $L = 1.1875$ (left) and $L = 0.9609375$ (right). The dot pattern emerges from $\beta = -1.5$ of (2.9). In contrast, the hexagonal pattern emerges from $\beta = 0.75$.

The hexagonal pattern and its inverse (dot pattern) were obtained as suggested by (2.8) and (2.9). Each pattern shown in Fig. 1 is linked to a positive and negative β, where β changes sign at $r = 2$ under the parameters. Kuto et al. [4] mentioned that the obtained hexagonal patterns are *inverse*, counter to the theoretical prediction; Theorem 2.2 implies that the hexagonal pattern emerges at a negative β and its inverse emerges at a positive β. Kuto et al. conjectured that the branch predicted from Theorem 2.2 is unstable and the pattern corresponding to a turned-back branch is stable. These results are consistent with the competition between expansion and contraction mentioned in Sec. 1. That is, a large r (an expansion effect larger than contraction) leads to a hexagonal spread of the living matter. In contrast, a small r (a contraction effect larger than expansion) leads to a dot aggregation. Note that the conjecture of stability is also justified by using a center manifold analysis [7].

4.2.2 3D:cubic-crystal pattern

The domain in this case was Ω_c, where the system size L was determined to obtain a crystal-like pattern at the first bifurcation. Similarly to in the above, $a_c(\boldsymbol{n}) \geq (\sqrt{r} + \sqrt{Dg})^2 / f := a_{\min}$, where $a_{\min}$ is attained at $L = \pi|\boldsymbol{n}| (D/rg)^{1/4}$ with $|\boldsymbol{n}|^2 = n_x^2 + n_y^2 + n_z^2$. Note that $|\boldsymbol{n}| = 1$ for SC, $|\boldsymbol{n}| = \sqrt{2}$ for BCC, and $|\boldsymbol{n}| = \sqrt{3}$ for FCC.

The cubic-crystal patterns (i.e., BCC, FCC, and SC) were obtained as shown in Figs. 2-5. Note that, for exhibiting the unit lattice of cubic crystals, the domain in the figures was extended to $\Omega_{c,2} = (0, 2L) \times (0, 2L) \times (0, 2L)$ in consideration of the reflection boundary. The BCC pattern has two types: regular BCC (Fig. 2) and its inverse (Fig. 3). It is proved that β for the BCC pattern changes sign at $r = 2$ under the parameters. The FCC (Fig. 4) and SC (Fig. 5) patterns have no inverses, i.e., $\beta = 0$. The difference originates from the existence or non-existence of a symmetry; i.e., an inverse pattern is obtained by the translation of the original for the FCC or SC pattern. The symmetry of the crystal determines the type of the bifurcation.

The stability of the 3D patterns has yet to be elucidated. First, the obtained BCC patterns are inverse, counter to the theoretical prediction. Note that the results are reasonable from the viewpoint of the competition between expansion and contraction: a small r indicating strong
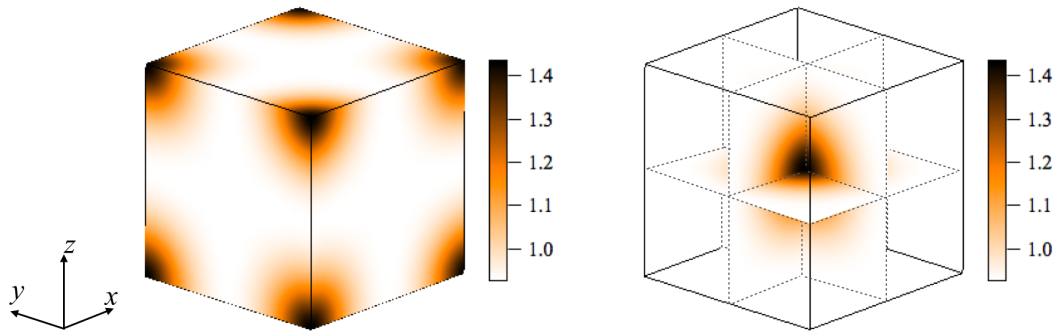
Figure 2: Overhead views of a steady-state BCC pattern in $\Omega_{c,2}$, where $L = 0.90625$ was set to obtain the pattern as the first bifurcation. Left and right represent color maps of u on the surface and on its inside cross-section, respectively. The parameters are $(a - a_c)/a_c \approx 0.002$, and $r = 1.0$ corresponding to $\beta = -0.5$.
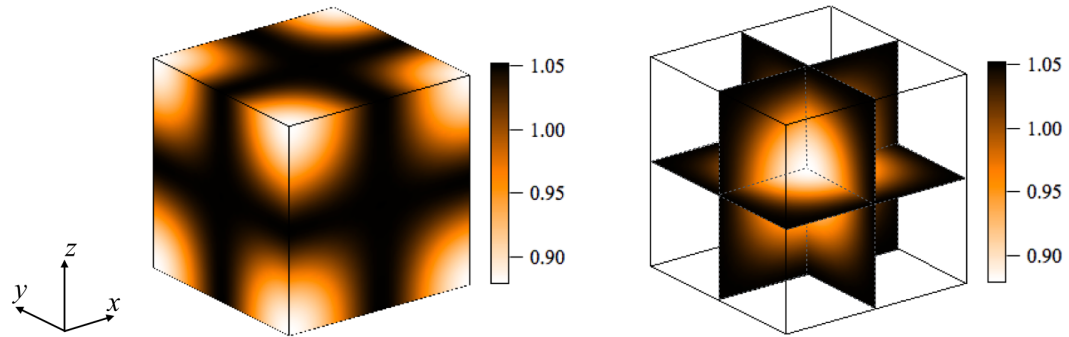

Figure 3: Overhead views of a steady-state pattern of inverse BCC in $\Omega_{c,2}$, where $L = 0.65625$ was set to obtain the pattern as the first bifurcation. Left and right represent color maps of u on the surface and on its inside cross-section, respectively. The parameters are $(a - a_c)/a_c \approx 0.002$, and $r = 3.5$ corresponding to positive $\beta = 0.75$.
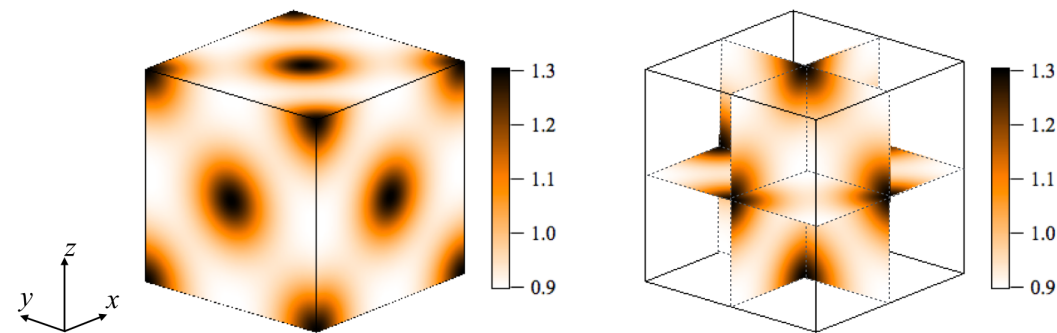

Figure 4: Overhead views of a steady-state FCC pattern in $\Omega_{c,2}$, where $L = 1.12500$ was set to obtain the pattern as the first bifurcation. Left and right represent color maps of u on the surface and on its inside cross-section, respectively. The parameters are $(a - a_c)/a_c \approx 0.002$ and $r = 1.0$.
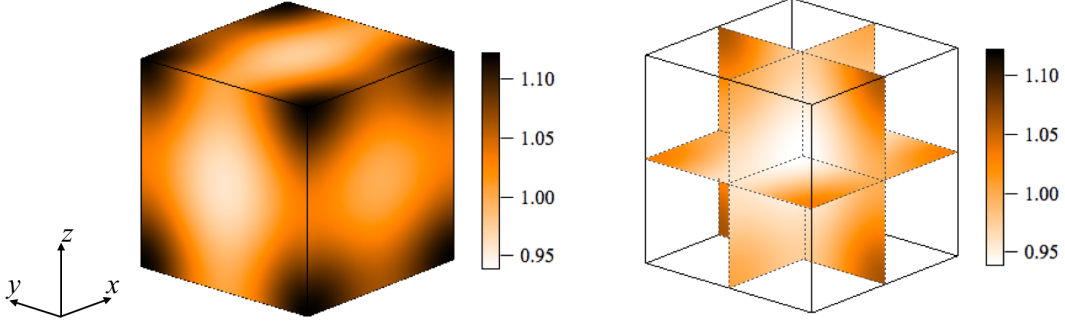
Figure 5: Overhead views of a transient SC pattern in $\Omega_{c,2}$, where $L = 0.65625$ was set to obtain the pattern as the first bifurcation. Left and right represent color maps of u on the surface and on its inside cross-section, respectively. The parameters are $(a - a_c)/a_c \approx 0.0003$ and $r = 1.0$. This result is at $t = 100$.
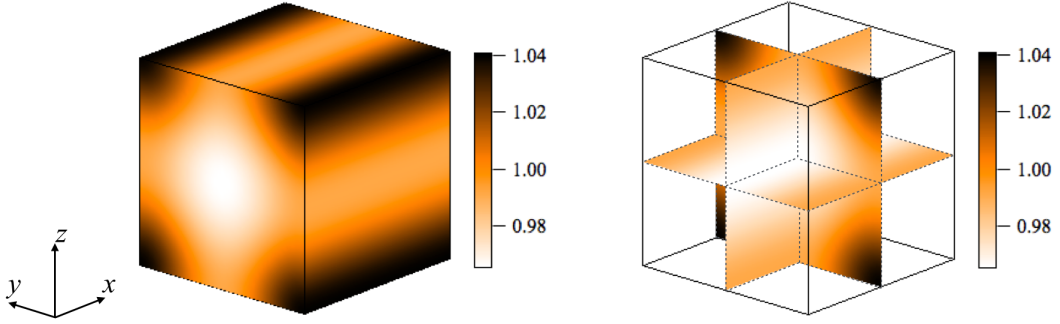

Figure 6: Overhead views of a pipe-like pattern in $\Omega_{c,2}$, where the parameters are the same as those of Fig. 5. Left and right represent color maps of u on the surface and on its inside cross-section, respectively. This result is at $t = 33800$ (steady state).

contraction leads to the spot pattern, and a large r indicating strong expansion does to the spread pattern. Second, although steady-state BCC (both faces) and FCC patterns were obtained, the SC pattern emerged only temporally around $t = 100$ and then converged to a pipe-like pattern as shown in Fig. 6. The stability of patterns should be examined by a center manifold analysis for 3D.

5   Summary

We have examined the chemotaxis and growth model introduced by Mimura and Tsujikawa. In a 2D rectangular domain, the hexagonal pattern and its inverse emerge, which is theoretically justified by the local bifurcation analysis. Although the patterns obtained by numerical calculations are inverse patterns, counter to the theoretical prediction, the patterns are reasonable from the viewpoint of the competition between spatial expansion and contraction of a living matter. In the 3D cubic domain, we have shown the cubic-crystal patterns FCC, SC, and BCC. The FCC

and SC patterns do not have solutions consisting of their inverse patterns, while the BCC pattern does. This difference originates from a symmetry inherent in each crystal, and determines the type of bifurcation. Furthermore, we have obtained the stable FCC and BCC patterns, but the SC pattern emerges only temporally. We will discuss the stability of the 3D crystal patterns elsewhere.

References

[1] T. Bánsági, V. K. Vanag, and I. R. Epstein, *Tomography of reaction-diffusion microemulsions reveals three-dimensional Turing patterns.*, Science 331 (2011), 1309–1312.

[2] M. G. Crandall and P. H. Rabinowitz, *Bifurcation from simple eigenvalues*, J. Funct. Anal. 340 (1971), 321–340.

[3] T. Hillen and K. J. Painter, *A user's guide to PDE models for chemotaxis.*, J. Math. Biol. 58 (2009), 183–217.

[4] K. Kuto, K. Osaki, T. Sakurai, and T. Tsujikawa, *Spatial pattern formation in a chemotaxis-diffusion-growth model*, Phys. D 241 (2012), 1629–1639.

[5] M. Mimura and T. Tsujikawa, *Aggregating pattern dynamics in a chemotaxis model including growth*, Phys. A 230 (1996), 499–543.

[6] T. Nishida, T. Ikeda, and H. Yoshihara, *Pattern formation of heat convection problems*, Lect. Notes Comput. Sci. Eng. 19 (2002), 209–218.

[7] T. Okuda and K. Osaki, *Bifurcation of hexagonal patterns in a chemotaxis-diffusion-growth system*, Nonlinear Anal. Real World Appl. 12 (2011), 3294–3305.

[8] H. Shoji and K. Saitoh, *Pattern formation in chemotaxic reaction-diffusion systems*, Int. J. Biomath. 5 (2012), 1260013-1–9.

[9] R. Strehl, A. Sokolov, D. Kuzmin, D. Horstmann, and S. Turek, *A positivity-preserving finite element method for chemotaxis problems in 3D*, J. Comput. Appl. Math. 239 (2013), 290–303.

Graduate School of Science and Technology
Kwansei Gakuin University
Sanda 669-1337, JAPAN
E-mail address: `narumi@kwansei.ac.jp`

関西学院大学・大学院理工学研究科 鳴海 孝之